Int. J. Nonlinear Anal. Appl. In Press, 1–11
ISSN: 2008-6822 (electronic)
http://dx.doi.org/10.22075/ijnaa.2023.27038.3487

Thermophoresis and Brownian motion effects on electrical magnetohydrodynamic flow of two-phase dissipative nanofluid with stratified boundary conditions

Dibyendu Saha, Anindita Mahanta, Dristi Rajbonshi, Sanjib Sengupta*

Department of Mathematics, Assam University, Silchar-788011, Assam, India

(Communicated by Javad Damirchi)

Abstract

This present paper reports the effect of thermophoresis and Brownian motion on the electrical magnetohydrodynamic (MHD) two-phase flow of nanofluid towards a linearly stretching sheet. The analysis is offered in cooperation with Joule heating, magnetic field, and chemical reaction. The flow model, represented by a highly nonlinear system of partial differential equations, is converted to dimensionless ordinary differential equations by introducing similarity transformations and then solved computationally using the optimal homotopy analysis method with the Mathematica package BVPh2.0, considering appropriate initial guesses and auxiliary linear operators. Behaviours of various variables affecting the flow, heat and mass transfer, and nanofluid volume fraction are analysed. Skin friction coefficient, local Nusselt number, and local Sherwood number are estimated and studied further. The results show that with increasing values of the thermophoresis parameter, the thermal boundary layer thickness increases near the wall. It is observed that higher values of the Brownian motion parameter tend to increase the fluid temperature profiles. It is also reported that larger values of the electric field parameter increase the local skin-friction coefficient significantly.

Keywords: thermophoresis, Brownian motion, MHD nanofluid, chemical reaction, viscous dissipation
2020 MSC: Primary 60J65; Secondary 76D50, 35Q35, 76W99

1 Introduction

The magnetohydrodynamic mixed convection flow of an electrically conducting nanofluid towards a stretching sheet and related study of heat and mass transfer has been an active area of research in recent times. The associated research has received great consideration due to its real-world applications in a variety of industries like plastic manufacturing, electronics, automotive, power, and aerospace industries, where there is a high demand for proficient heat exchanger devices. Nanofluids [7] are then used for heat transfer enhancement (by 15% to 40%) as compared to conventional base fluids like water and ethylene glycol. The heat transfer improvement is caused by to suspension of ultra-fine nanoparticles in the base fluids. Recently, heat and mass transfer characteristics on the mixed convection flow have been analyzed, and noteworthy findings are reported by [21].

*Corresponding author
Email addresses: saha9737@gmail.com (Dibyendu Saha), mahantaofficial27@gmail.com (Anindita Mahanta), dristirajbonshi2017@gmail.com (Dristi Rajbonshi), sanjib_aus2009@rediffmail.com (Sanjib Sengupta)

Received: May 2022 *Accepted:* October 2023

The stretching boundary flow problems have notable coverage in the extrusion process of the metal industries. The study of MHD nanofluid with stretching boundary layer finds direct applications in the field of engineering and technology, like in the polymer industry, optical grating, and optical switches. The quality of the final products greatly depends on the cooling and stretching rates, with certain characteristics. MHD Williamson nanofluid flow over a stretching sheet under various effects is solved in [6]. The results disclose that the velocity distribution of the fluid is negatively affected by the influence of the magnetic field parameter. Various aspects of MHD flow past a vertical flat surface and heat and mass transfer study thereof is done by [20, 18]. Interesting outcomes are reported in the thermal energy investigation of MHD nano-material liquid flow [5]. [12] investigated the combined impact of nonlinear radiation and magnetic field on three-dimensional rotational nanofluid flow.

The heat and mass transfer problems of MHD nanofluid flow under the influence of chemical reaction have rich applications in industries like spraying drying of milk, energy transfer in the wet cooling tower, and evaporation processes. The effect of chemical reaction parameters on the MHD flow of nanofluid under different physical situations is considered by [8, 19, 16]. The results reveal that larger values of the chemical reaction parameter weaken the nanoparticle concentration. It is also found from the study [9] that temperature improves with more joule heating, and in the presence of a magnetic field, the Joule heating strongly develops the temperature field. The chemical reaction effect on unsteady electrical MHD flow of nanofluid is studied by [10]. Analysis of the chemical reaction effect done by [2] is worth mentioning here.

Brownian motion of suspended nanoparticles in base fluids with constant temperature gradient produces to crucial thermophoresis. At a higher temperature of the traditional fluid, the dispersion of particles is greater, and the Brownian force is greater. Due to the temperature gradient in the dispersion flow regime, minor particles disperse faster in the hotter domain and slower in the colder domain; as a result, nanoparticles migrate from a hotter to a colder region in the fluid. Nanoparticles motion on average against the gradient resulted from the temperature gradient. The average motion of these nanoparticles is known as thermophoresis. Thermophoresis, together with magnetic field and Joule heating, improves the temperature field and increases the thermal boundary layer thickness [1]. Also, thermophoresis decreases the Nusselt number [15]. Detailed reports of thermophoresis and Brownian effect on MHD nanofluid can be found in [4]. Further studies are reported in [11].

Stratification of fluids is a natural process that is nothing but the formation of layers and occurs due to temperature differences and concentration differences. Stratification generates a transition zone of a temperature gradient between the hotter and colder regions of the fluid. Thermal stratification is prominent for its implications in solar engineering as it can forecast the possibilities of realizing higher energy efficiency. Results of [14] show that an increase in thermal stratification decreases the wall temperature, and it has a significant effect on the temperature distribution in the flow near the wall. The results of [17] study the impact of the Hall current on Jeffrey nanofluid flow in a rotating frame.

Most of the explorations on MHD mixed convection flow of nanofluid towards a stretching sheet and heat transfer with effects of Brownian motion do not incorporate the combined effect of thermophoresis and Brownian motion together with chemical reaction effect on two-phase double diffusive MHD flow past a stretching sheet embedded in a thermally stratified medium in the presence of both thermal stratification and solutal stratification, and also in attendance of electric field. This analysis is carried out to fill such a gap.

2 Mathematical Analysis

The schematic sketch of the flow model is represented in Figure 1. The coordinate system of the flow is considered in such a way that the y-axis is measured along the stretching sheet, and the z-axis is normal to it. The flow is occupied above the surface $z > 0$. The magnetic and electric fields obey Ohm's law, defined by $\overrightarrow{J} = \sigma(\overrightarrow{E} + \overrightarrow{q} \times \overrightarrow{B})$, where $\overrightarrow{J}$ is the Joule current, $\overrightarrow{E}$ is the electric field intensity vector, $\overrightarrow{q}$ is the charge of electrons, $\overrightarrow{B}$ is the magnetic field vector. The induced magnetic field and Hall current effects are insignificant for the small magnetic Reynolds number. The governing equations of the flow, which are formulated based on Maxwell's equations and Ohm's law, are given as:

$$\frac{\partial v}{\partial y} + \frac{\partial w}{\partial z} = 0 \tag{2.1}$$

$$\begin{aligned}\rho_f\Big(\frac{\partial v}{\partial t} + v\frac{\partial v}{\partial y} + w\frac{\partial v}{\partial z}\Big) =& \mu\frac{\partial^2 v}{\partial z^2} - \sigma {B^*}_0(E^*{}_0 + v{B^*}_0 \sin\omega)\sin\omega \\ &+ \Big[(1-\varphi_\infty)\rho f_\infty\Big\{\beta_T\big(T-T_\infty\big) + \beta_C\big(C-C_\infty\big)\Big\} - \big(\rho_s - \rho f_\infty\big)\big(\varphi-\varphi_\infty\big)\Big]g\end{aligned} \tag{2.2}$$

$$(\rho c)_f\Big(\frac{\partial T}{\partial t}+v\frac{\partial T}{\partial y}+w\frac{\partial T}{\partial z}\Big)=K\Big(\frac{\partial^2 T}{\partial z^2}\Big)+\mu\Big(\frac{\partial v}{\partial z}\Big)^2+\tau(\rho c)_f\Big\{D_B\frac{\partial \varphi}{\partial z}\frac{\partial T}{\partial z}+\frac{D_T}{T_\infty}\Big(\frac{\partial T}{\partial z}\Big)^2\Big\}+\frac{D_M K_T}{C_s C_p}\frac{\partial^2 C}{\partial z^2}$$
$$+Q_a(\rho c)_f(C-C_\infty) \quad (2.3)$$

$$\frac{\partial C}{\partial t}+v\frac{\partial C}{\partial y}+w\frac{\partial C}{\partial z}=D_M\frac{\partial^2 C}{\partial z^2}+\frac{D_M K_T}{T_M}\frac{\partial^2 T}{\partial z^2}-k_l(C-C_\infty) \quad (2.4)$$

$$\frac{\partial \varphi}{\partial t}+v\frac{\partial \varphi}{\partial y}+w\frac{\partial \varphi}{\partial z}=D_B\frac{\partial^2 \varphi}{\partial z^2}+\frac{D_T}{T_\infty}\frac{\partial^2 T}{\partial z^2}, \quad (2.5)$$

where the magnetic field factor is $B^*{}_0 = B_0/\sqrt{(1-\delta t)}$, and $E^*{}_0 = E_0/\sqrt{(1-\delta t)}$ is the electrical field factor. $\tau = (\rho c)_s/(\rho c)_f$ denotes the ratio between the effective heat transfer capacity of the ultrafine nanoparticle material and the heat capacity of the fluid. The boundary conditions defined for the physical situation are presented as:

$$v = v_w(y,0,t)=\frac{a}{1-\delta t}y, \quad w = w_w(y,0,t)=-\frac{w_0}{\sqrt{1-\delta t}}, \quad T = T_w(y,0,t)=T_0+\frac{A_1}{1-\delta t}y,$$
$$C = C_w(y,0,t)=C_0+\frac{B_1}{1-\delta t}y, \quad \varphi=\varphi_w(y,0,t)$$
$$v(y,\infty,t)=0, \quad T(y,\infty,t)=T_\infty=T_0+\frac{A_2}{1-\delta t}y, \quad C(y,\infty,t)=C_\infty=C_0+\frac{B_2}{1-\delta t}y, \quad \varphi(y,\infty,t)=\varphi_\infty \quad (2.6)$$

where, $\delta t < 1$ and the constants A_1, A_2, B_1, B_2 are constants and varied to alter the intention of the stratification in the medium.

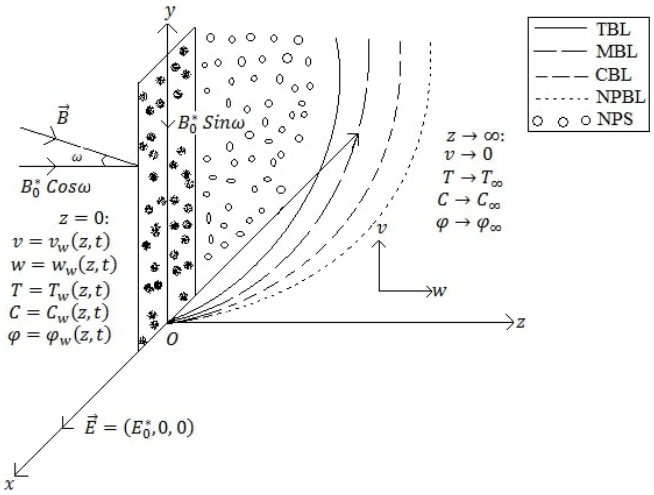

Figure 1: Schematic representation of the flow model

To obtain similarity solution of (2.1) to (2.5) based on the boundary requirements (2.6), the non-dimensional variables are presented as:

$$\psi = \sqrt{\frac{a\nu}{1-\delta t}}yf(\eta), \quad \eta = \sqrt{\frac{a\nu}{\nu(1-\delta t)}}z, \theta(\eta) = \frac{T-T_\infty}{T_w-T_0}, \quad \xi(\eta) = \frac{C-C_\infty}{C_w-C_0}, \quad \chi(\eta) = \frac{\varphi-\varphi_\infty}{\varphi_w-\varphi_\infty}. \quad (2.7)$$

The stream function ψ can be defined as:

$$v=\frac{\partial \psi}{\partial z}, \quad w=-\frac{\partial \psi}{\partial y}. \quad (2.8)$$

Now, applying (2.7) and (2.8) into (2.2) to (2.5) and boundary conditions (2.6), the dimensionless equations of momentum, energy, nanoparticle concentration and nanoparticle volume fraction are as follows:

$$f'''-\Lambda\Big(f'+\frac{\eta}{2}f''\Big)+ff''-M(E_p+f'\sin\omega)\sin\omega+\lambda(\theta+B_p\xi-B_n\chi)=0 \quad (2.9)$$

$$\frac{1}{Pr}\theta'' + f\theta' + N_b\theta'\chi' + N_t\theta'^2 + Du\xi'' - \Lambda\frac{\eta}{2}\theta' + Ecf''^2 + R_a\xi = 0 \tag{2.10}$$

$$\frac{1}{Sc}\xi'' - \Lambda\frac{\eta}{2}\xi' + f\xi' + Sr\theta'' - Cr\xi = 0 \tag{2.11}$$

$$\chi'' - Pr\,Le\Big(\Lambda\frac{\eta}{2} - f\Big)\chi' + \frac{N_t}{N_b}\theta'' = 0 \tag{2.12}$$

Together with the boundary conditions defined as:

$$\begin{aligned} &f(0) = s, \quad f'(0) = 1, \quad \theta(0) = 1 - S_t, \quad \xi(0) = 1 - S_c, \quad \chi(0) = 1 \\ &f'(\infty) = 0, \quad \theta(\infty) = 0, \quad \xi(\infty) = 0, \quad \chi(\infty) = 0 \end{aligned} \tag{2.13}$$

Here, $\Lambda = \delta/a$, $M = \big(\sigma B_0^2/(a\rho_f)\big)$, $E_p = E_0/(B_0 v_w)$, $\lambda = Gr/Re^2$ ($\lambda > 0$: heated surface, and $\lambda < 0$: cold surface), $Gr = g\rho_{f\infty}\beta_T(T_w - T_0)(1-\varphi_\infty)/\big(\nu^2\rho_f\big)$, $Re = a^2y/\big\{\nu^2(1-\delta t)^2\big\}$. Again, $B_p = \beta_C(C_w - C_0)/\big\{\beta_T(T_w - T_0)\big\}$, $B_n = (\rho_s - \rho_{f\infty})(\varphi_w - \varphi_\infty)/\big\{\rho_{f\infty}\beta_T(T_w - T_0)(1-\varphi_\infty)\big\}$, $Pr = \nu/\alpha$, $N_b = \tau D_B(\varphi_w - \varphi_\infty)/\nu$, $N_t = \tau D_T(T_w - T_0)/(\nu T_\infty)$, $Du = D_M K_T(C_w - C_0)/\big\{\nu(\rho c)_f C_s C_p(T_w - T_0)\big\}$, $Ec = {v_w}^2/\big\{C_p(T_w - T_0)\big\}$, $R_a = Q_a(C_w - C_0)/(T_w - T_0)$, $Sc = \nu/D_M$, $Sr = D_M K_T(T_w - T_0)/\big\{\nu T_M(C_w - C_0)\big\}$, $Cr = k_l/a$, $Le = \alpha/D_M$, $s = w_0/\sqrt{a\nu}$ (> 0), $S_t = A_2/A_1$, and $S_c = B_2/B_1$.

The skin-friction coefficient, the local Nusselt number, and the local Sherwood number are:

$$c_f = \frac{\tau_w}{\frac{1}{2}\rho v_w^2}, \quad Nu = \frac{yq_w}{k(T_w - T_0)}, \quad Sh = \frac{yj_w}{D_M(C_w - C_0)}, \tag{2.14}$$

where,

$$\tau_w = \mu\left(\frac{\partial v}{\partial z}\right)_{z=0}, \quad q_w = -k\left(\frac{\partial T}{\partial z}\right)_{z=0}, \quad j_w = -D_M\left(\frac{\partial C}{\partial z}\right)_{z=0}. \tag{2.15}$$

The local skin-friction coefficient, the local Nusselt number, and the local Sherwood numbers are presented in non-dimensional form as:

$$(Re)^{\frac{1}{2}}c_f = 2f''(0), \quad (Re)^{-\frac{1}{2}}Nu = -\theta'(0), \quad (Re)^{-\frac{1}{2}}Sh = -\xi'(0). \tag{2.16}$$

3 Computational Solutions by OHAM

The solution of the coupled nonlinear equations (2.9) to (2.12) together with the boundary conditions (2.13) is computed in series form with the optimal homotopy analysis method (OHAM). OHAM is a convenient and powerful mathematical tool for solving highly nonlinear problems. The method is best suited for the studied problem as high-order approximations can be obtained by this tool with much less effort when compared to the traditional HAM. Also, OHAM is imported when compared to other methods, due to its readiness in solving complex nonlinear systems and as less computational time is required. The appropriate initial guesses are made as follows:

$$f_0(\eta) = s + 1 - e^{-\eta}, \quad \theta_0(\eta) = (1 - S_t)e^{-\eta}, \quad \xi_0(\eta) = (1 - S_c)e^{-\eta} \quad \text{and} \quad \chi_0(\eta) = e^{-\eta}. \tag{3.1}$$

Also, the auxiliary linear operators for this problem are as follows:

$$L_f(\eta) = f''' - f', \quad L_\theta(\eta) = \theta'' - \theta', \quad L_\xi(\eta) = \xi'' - \xi' \quad \text{and} \quad L_\chi(\eta) = \chi'' - \chi'. \tag{3.2}$$

3.1 Optimal convergence control parameters

The auxiliary parameters which are involved in the convergence of the homotopic solutions are c_0^f, c_0^θ, c_0^ξ, and c_0^χ [6]. We have used the Mathematica package BVPh2.0 to determine the convergence control parameters by minimizing the average residual errors. It is observed that the optimum convergence control parameter with minimum average residual errors is achieved in the 4th iteration.

4 Results and Discussion

The impacts of different important physical parameters are depicted in this section through numerical and graphical results of the discussed flow model.

The effects of Brownian motion parameter (N_b) on temperature and volume fraction profiles are presented in Figure 2 and Figure 3, respectively. N_b appears as the coefficient of a mixed derivative term in the dimensionless temperature equations and as a coefficient of a second-order temperature derivative term in the non-dimensional nanoparticle volume fraction equation. N_b is the fundamental parameter which commands diffusion of nanoparticles and with an improvement in the values of N_b, nanoparticle fraction profiles strongly decline, as seen in Figure 3, whereas the temperature profiles increase significantly, as being a two-phase fluid, the suspended nanoparticles move randomly and thus enhances energy exchange rates, as observed in Figure 2. The influence of thermophoresis parameter (N_t) on temperature and nanoparticle fraction profiles is described in Figure 4 and Figure 5. As is the case with N_b, the thermophoresis parameter also features in both dimensionless temperature and nanoparticle fraction equations. With an increase in the values of N_t, a slight increase in the temperature profiles is observed near the wall at $\eta = 0$, but as η is increased further, a switch is observed and temperature profiles decrease. Because of the thermophoresis, an additional amount of heat is produced with the contact of the base fluid with the nanoparticles. Consequently, the thermal boundary layer gets thicker and intense particles are dragged from the hotter to the colder surface region for thermophoresis, raising the fluid temperature near the plate. But a reverse phenomenon appears in the free stream region or far from the plate, resulting in the reduction of the fluid temperature. Also, nanoparticle fraction profiles are seen to be enhanced with increasing values of N_t throughout the range.

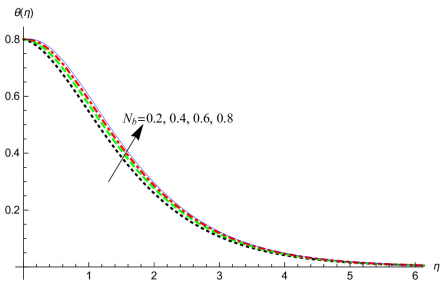

Figure 2: Influence of Brownian motion parameter on the temperature profile

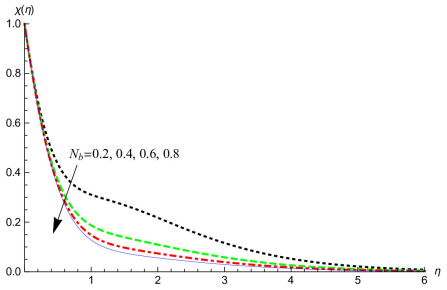

Figure 3: Influence of Brownian motion parameter on the volume fraction profile

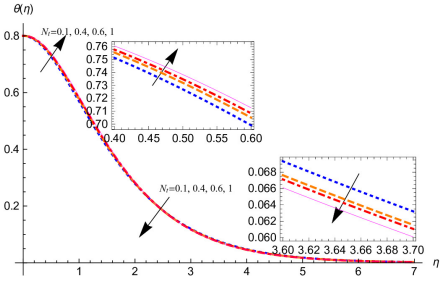

Figure 4: Influence of thermophoresis parameter on the temperature profile

Figure 6 exhibits the effect of Dufour number (Du) on the temperature profiles. The Dufour number is defined as the ratio of the concentration difference to the temperature difference. So, with higher values of Du, the thermal and solutal buoyancy forces improve the convective velocity and consequently, the temperature profiles are increased.

Figure 7 shows the impact of chemical reaction parameter (Cr) on the concentration profiles. With higher values of, the transport of molar species from the high concentration zone (plate region) to the low concentration zone (free-stream region) increases, which reduces the growth of the concentration boundary layer and thus lowers the concentrations near the plate region. Due to the dilution of concentrations near the plate region, the effect of mass buoyancy force minimizes. It is evident that the destructive chemical rate ($Cr > 0$) enhances the mass transfer rate and consequently a decline in nanoparticle concentration. The effect of Lewis number (Le) on the nanoparticle fraction profile is described in Figure 8. As the mass transfer rate is sensitive to the increasing values of Lewis number, this reduces the concentration profile and consequently, the nanoparticle fraction profile also reduces, as depicted in Figure 8.

Figure 9, Figure 10, and Figure 11 are sketched to analyze the variation of the velocity, temperature, and nanoparticle volume fraction profiles, respectively, for varying thermal stratification parameter (S_t). As shown in Figure 9 and Figure 10, the fluid velocity and fluid temperature profiles decrease for increasing values of the thermal stratification parameter. The fluid temperature is a decreasing function of thermal stratification, so fluid temperature and thermal boundary layer thickness strongly reduce with increasing values of the thermal stratification parameter. Thus, the rate of heat transfer increases for higher values of S_t. Also, the nanoparticle fraction profile got reduced for advanced values of S_t as observed in Figure 11. Figure 12 aimed to shed light on the fluid temperature profile for enhancing values of the solutal stratification parameter (S_c). It is witnessed that the temperature profile got reduced for higher values of S_c. The temperature flow pattern is seen to be uniformly decreasing with increasing dimensionless transverse coordinate η.

Figure 13 and Figure 14 display the effect of mixed convection parameter (λ) on the fluid velocity and velocity

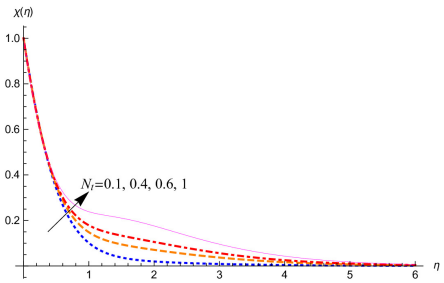

Figure 5: Influence of thermophoresis parameter on the volume fraction profile

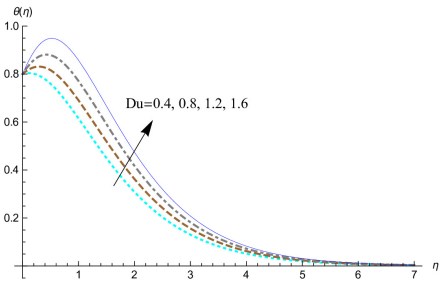

Figure 6: Influence of Dufour number on the temperature profile

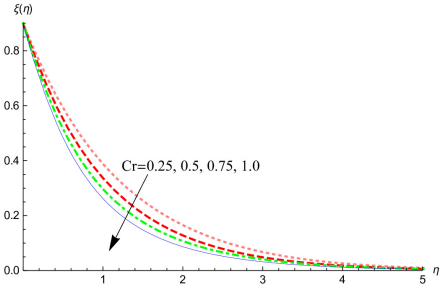

Figure 7: Influence of chemical reaction parameter on the concentration profile

temperature profiles, respectively. The velocity profiles advance uniformly for advancing values of λ, whereas reverse phenomena are observed for temperature profiles, as it decreases with increasing values of λ.

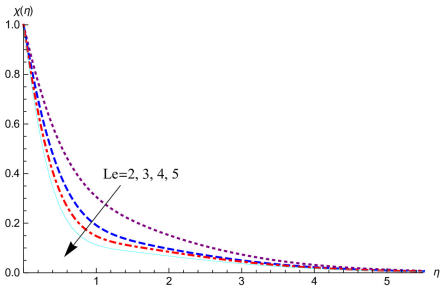

Figure 8: Influence of Lewis number on the volume fraction profile

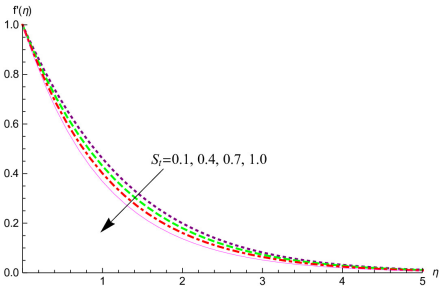

Figure 9: Influence of thermal stratification on the velocity profile

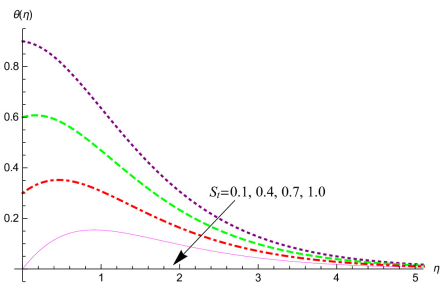

Figure 10: Influence of thermal stratification on the temperature profile

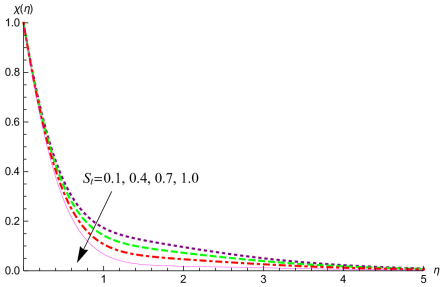

Figure 11: Influence of thermal stratification on the volume fraction profile

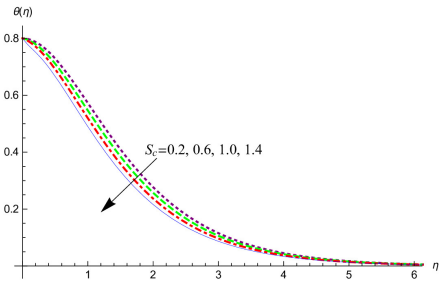

Figure 12: Influence of solutal stratification on the temperature profile

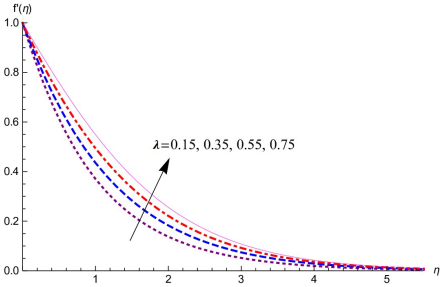

Figure 13: Influence of mixed convection parameter on the velocity profile

Figure 15 and Figure 16 present the effect of the unsteadiness parameter (Λ) on the fluid velocity and temperature profiles, respectively. It is observed that both fluid velocity and fluid temperature increase for increasing values of Λ. The influence of magnetic field parameter (M) on fluid velocity profiles is depicted in Figure 17. It is seen that the velocity profiles decrease with increasing strength of the magnetic field effect, applied normally to the fluid flow. The magnetic field produces a resistive force known as the Lorentz force in the free convection region along the axial direction, which opposes the flow. As this force acts as an obstruction to the flow, it subsequently extends the boundary layer thickness all over the flow regime. It can also be observed that the effect of the magnetic field is much stronger near the surface of the plate. Figure 18 demonstrates the effect of nanoparticle buoyancy ratio (B_p) over the fluid velocity, and it is observed that the fluid velocity is increased with increasing values of B_p.

Table 1 displays the variation of local Nusselt and Sherwood numbers for different values of the thermophoresis parameter, thermal, and solutal stratification parameters. It is observed that the local Nusselt number decreases with increasing N_t and S_t but increases with increasing S_c. The Sherwood number increases with increasing Nt but decreases with increasing S_t and S_c.

Table 2 displays the variation of the local skin friction coefficient for different parametric values. It is noticed from the table that the local skin friction coefficient increases with increasing magnetic field parameter, inclination angle,

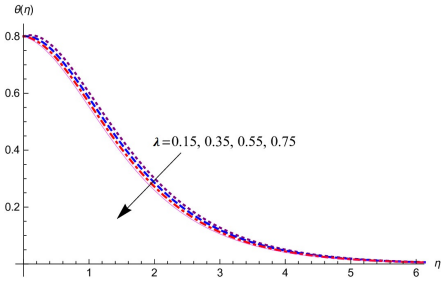

Figure 14: Influence of mixed convection parameter on the temperature profile

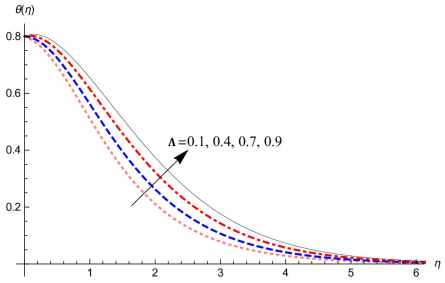

Figure 15: Influence of unsteadiness parameter on the temperature profile

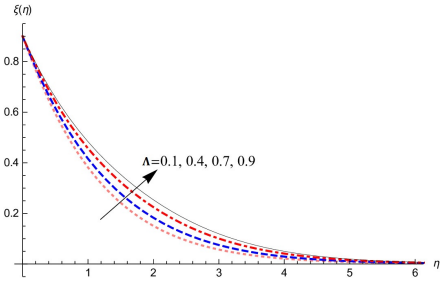

Figure 16: Influence of unsteadiness parameter on the concentration profile

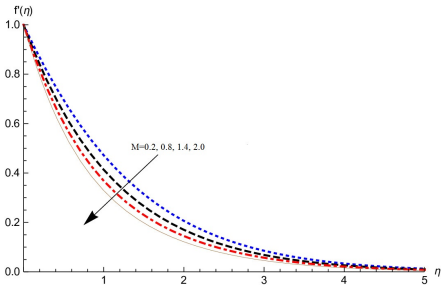

Figure 17: Influence of magnetic filed parameter on the velocity profile

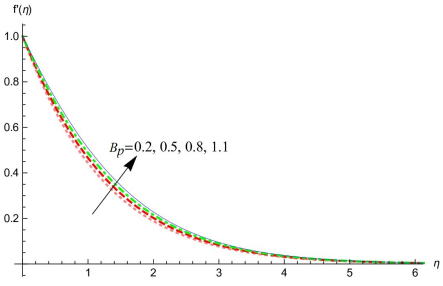

Figure 18: Influence of nanoparticle buoyancy ratio parameter on the velocity profile

and electric field parameter. But, decreases with increasing nanofluid buoyancy ratio.

Table 3 shows the numerical comparison of values of local Nusselt number of the present result with the results of [13] and [3] under limiting conditions. It is observed that our solution has excellent agreement with the existing numerical solution.

Table 1: Numerical values for local Nusselt and Sherwood number for different parametric values

N_t	S_t	S_c	$-\theta'(0)$	$-\xi'(0)$
0.1	0.2	0.1	0.008092920	0.6299865
0.2			0.004805638	0.6307804
0.3			0.001435349	0.6320616
0.5	0.05		0.05829204	0.6343520
	0.1		0.03769773	0.6341346
	0.15		0.01675675	0.6339904
	0.2	0.2	0.005648488	0.5660132
		0.3	0.01579379	0.4982123
		0.4	0.02590387	0.4308101

5 Conclusions

The modelled two-phase flow of electrically conducting MHD nanofluid flow through a linearly stretching sheet is investigated under thermophoresis and Brownian motion effects. The nonlinear system of equations of the considered flow model is solved computationally by OHAM. The present model shows excellent agreement with earlier findings. The influences of different interesting parameters of engineering interests on the fluid velocity, temperature, concentration, and nanoparticle volume fraction are summarized as follows:

- Velocity field rises with an increase in the values of mixed convection parameter, unsteadiness parameter, and nanoparticle buoyancy ratio, but decreases for increasing values of thermal stratification parameter and magnetic field parameter.

Table 2: Numerical values for local skin-friction coefficient for different parametric values

M	ω	E_p	Nc	$2f''(0)$
0.6	$\pi/4$	0.01	0.3	1.6330272
0.8				1.7432142
1.0				1.8484652
0.4	$5\pi/18$			1.5576154
	$6\pi/18$			1.6313752
	$7\pi/18$			1.6897402
	$\pi/4$	0.03		1.5298216
		0.06		1.5485148
		0.09		1.5671596
		0.01	0.2	1.5604630
			0.5	1.4314246
			0.8	1.3034674

Table 3: Comparison of results for the local Nusselt number

Pr	**Present results**	**Khan and Pop [13]**	**Akbar et al. [3]**
0.07	0.066296	0.0663	0.0656
0.20	0.169105	0.1691	0.1691
0.70	0.453912	0.4539	0.4539
2.0	0.911286	0.9113	0.9114
7.0	1.895365	1.8954	1.8954
20.0	3.353908	3.3539	3.3539
70.0	6.462117	6.4621	6.4622

- Temperature field and thermal boundary layer thickness are increasing functions of Brownian motion parameter, Dufour number, and unsteadiness parameter, whereas, reverse phenomena are observed for thermal stratification parameter, solutal stratification parameter, and mixed convection parameter.
- Nanofluid concentration field and concentration boundary layer thickness decrease with an increase in parametric values of the chemical reaction.
- Nanoparticle volume fraction profiles decline with increasing values of Brownian motion parameter, Lewis number, and thermal stratification parameter.
- With increasing values of the thermophoresis parameter, the thermal boundary layer thickness increases near the wall but decreases far from the plate, and the nanoparticle fraction profile increases.
- Local Nusselt number decreases and Sherwood number increases with increasing thermophoresis parameter. The local skin friction coefficient increases with increasing electric field parameter.

6 Nomenclature

Roman letters

B_0	Magnetic field factor [N·A^{-1}m^{-1}]
E_0	Electric field factor [N·C^{-1}]
v	Velocity component along y-axix [m·s^{-1}]
w	Velocity component along z-axis [m·s^{-1}]
T	Temperature of fluid [K]
C	Concentration of fluid [mol·m^{-3}]

t	Time variable [s]
g	Gravitational acceleration [m·s^{-2}]
K	Thermal conductivity [W·m^{-1}K^{-1}]
D_B	Brownian diffusion coefficient [m^{2}S^{-1}]
D_T	Thermophoresis diffusion coefficient [m^{2}s^{-1}]
D_M	Species diffusivity [m^{2}s^{-1}]
K_T	Thermal diffusivity ratio [m^{2}s^{-1}]
C_s	Concentration susceptibility [m^{3}kg^{-1}]
C_p	Specific heat at constant pressure [J · kg^{-1}K^{-1}]
Q_a	Radiation absorption parameter
k_l	First order chemical reaction parameter
a	Positive constant
f	Dimensionless velocity
M	Magnetic field parameter
E_p	Electric field parameter
B_p	Nanoparticles buoyancy ratio
B_n	Nanofluid buoyancy ratio
Pr	Prandtl number
N_b	Brownian motion parameter
N_t	Thermophoresis parameter
Du	Dufour number
Ec	Eckart number
R_a	Radiation absorption parameter
Sc	Schmidt number
Sr	Soret number
Cr	Chemical reaction parameter
Le	Lewis number
s	Suction parameter
S_t	Thermal stratification parameter
S_c	Solutal Stratification parameter
Gr	Thermal Grashof number
Re	Reynolds number
q_w	Surface heat flux [W·m^{-2}]
j_w	Surface mass flux [kg·m^{-2}s^{-1}]

Greek letters

σ	Electrical conductivity [S·m^{-1}]
φ	Nanoparticle volume fraction
ρ	Density of fluid [kg·m^{-3}]
μ	Dynamic viscosity [N·S·m^{-2}]
ω	Inclination angle of stretching sheet with magnetic field factor [rd]
β	Volumetric expansion coefficient [K^{-1}]
δ	Positive constant
ψ	Stream function
ν	Kinematic coefficient of viscosity [m^{2}s^{-1}]
η	Similarity independent variable
θ	Dimensionless temperature
ξ	Dimensionless concentration
χ	Dimensionless nanoparticle volume fraction
Λ	Unsteadiness parameter
λ	Mixed convection parameter
τ_w	Shear stress in stretching sheet [N·m^{-2}]

Subscripts

T	Related to thermal properties

C	Related to concentration properties
f	Condition of base fluid
s	Condition of suspended nanoparticles
0	Reference condition
w	Wall condition
∞	Ambient condition

References

[1] N.Y. Abd Elazem, *Numerical results for influence the flow of MHD nanofluids on heat and mass transfer past a stretched surface*, Nonlinear Engin. **10** (2021), no. 1, 28–38.

[2] A.A. Afify, *MHD free convective flow and mass transfer over a stretching sheet with chemical reaction*, Heat Mass Transfer **40** (2004), no. 6, 495–500.

[3] N. Akbar, Z. Khan, S. Nadeem, and W. Khan, *Double-diffusive natural convective boundary-layer flow of a nanofluid over a stretching sheet with magnetic field*, Int. J. Numer. Meth. Heat Fluid Flow **26** (2016), no. 1, 108–121.

[4] M. Arshad, A. Hussain, A. Hassan, Q. Haider, A.H. Ibrahim, M.S. Alqurashi, A.H. Almaliki, and A. Abdussattar, *Thermophoresis and Brownian effect for chemically reacting magneto-hydrodynamic nanofluid flow across an exponentially stretching sheet*, Energies **15** (2021), no. 1, 143.

[5] M. Arshad, A. Hussain, A. Hassan, P. Wróblewski, A. Elfasakhany, M.A. Elkotb, M.A.H. Abdelmohimen, and A.M. Galal, *Thermal energy investigation of magneto-hydrodynamic nano-material liquid flow over a stretching sheet: Comparison of single and composite particles*, Alexandria Engin. J. **61** (2022), no. 12, 10453–10462.

[6] J. Bouslimi, M. Omri, R.A. Mohamed, K.H. Mahmoud, S.M. Abo-Dahab, M.S. Soliman, *MHD Williamson nanofluid flow over a stretching sheet through a porous medium under effects of joule heating, nonlinear thermal radiation, heat generation/absorption, and chemical reaction*, Adv. Math. Phys. **2021** (2021), no. 1, 9950993.

[7] S.U.S. Choi and J.A. Eastman, *Enhancing thermal conductivity of fluids with nanoparticles*, Tech. Report, Argonne National Lab. (ANL), Argonne, IL (United States), 1995.

[8] Y.S. Daniel, Z. Abdul Aziz, Z. Ismail, and F. Salah, *Entropy analysis in electrical magnetohydrodynamic (MHD) flow of nanofluid with effects of thermal radiation, viscous dissipation, and chemical reaction*, Theor. Appl. Mech. Lett. **7** (2017), no. 4, 235–242.

[9] Y.S. Daniel, Z. Abdul Aziz, Z. Ismail, and F. Salah, *Impact of thermal radiation on electrical mhd flow of nanofluid over nonlinear stretching sheet with variable thickness*, Alexandria Engin. J. **57** (2018), no. 3, 2187–2197.

[10] Y.S. Daniel, Z. Abdul Aziz, Z. Ismail, and F. Salah, *Thermal radiation on unsteady electrical MHD flow of nanofluid over stretching sheet with chemical reaction*, J. King Saud Univ.-Sci. **31** (2019), no. 4, 804–812.

[11] A. Hussain, M. Arshad, A. Hassan, A. Rehman, H. Ahmad, J. Baili, and T.N. Gia, *Heat transport investigation of engine oil based rotating nanomaterial liquid flow in the existence of partial slip effect*, Case Stud. Thermal Engin. **28** (2021), 101500.

[12] A. Hussain, M. Abdelghany Elkotb, M. Arshad, A. Rehman, K. Sooppy Nisar, A. Hassan, and C.A. Saleel, *Computational investigation of the combined impact of nonlinear radiation and magnetic field on three-dimensional rotational nanofluid flow across a stretchy surface*, Processes **9** (2021), no. 8, 1453.

[13] W.A. Khan and I. Pop, *Boundary-layer flow of a nanofluid past a stretching sheet*, Int. J. Heat Mass Transfer **53** (2010), no. 11-12, 2477–2483.

[14] O.K. Koriko, I.L. Animasaun, A.J. Omowaye, and T. Oreyeni, *The combined influence of nonlinear thermal radiation and thermal stratification on the dynamics of micropolar fluid along a vertical surface*, Multidis. Mod. Mater. Struct. **15** (2019), no. 1, 133–155.

[15] J.V. Ramana Reddy, V. Sugunamma, and N. Sandeep, *Thermophoresis and Brownian motion effects on unsteady MHD nanofluid flow over a slendering stretching surface with slip effects*, Alexandria Engin. J. **57** (2018), no. 4, 2465–2473.

[16] N.N. Reddy, V.S. Rao, and B.R. Reddy, *Chemical reaction impact on MHD natural convection flow through porous medium past an exponentially stretching sheet in presence of heat source/sink and viscous dissipation*, Case Stud. Thermal Engin. **25** (2021), 100879.

[17] D. Saha and S. Sengupta, *Dual DTM-Padé approximations on free convection MHD mass transfer flow of nanofluid through a stretching sheet in presence of Soret and Dufour phenomena*, WSEAS Trans. Fluid Mech **15** (2020), 23–40.

[18] S. Saleem, H. Rafiq, A. Al-Qahtani, M. Abd El-Aziz, M.Y. Malik, I.L. Animasaun, *Magneto Jeffrey nanofluid bioconvection over a rotating vertical cone due to gyrotactic microorganism*, Math. Prob. Engin. **2019** (2019), 3478037.

[19] P.V. Satya Narayana, N. Tarakaramu, and D. Harish Babu, *Influence of chemical reaction on MHD couple stress nanoliquid flow over a bidirectional stretched sheet*, Int. J. Ambient Energy **43** (2022), no. 1, 4928–4938.

[20] S. Sengupta, *Heat and Mass Transfer Phenomena in MHD Flow: Modelling with Applications*, Scientific Research Publishing, Inc., USA, 2014.

[21] S. Sengupta and A. Karmakar, *Heat and mass transfer analysis on MHD mixed convection flow of radiative chemically heat generating fluid with viscous dissipation and thermo-diffusion effect*, Front. Heat Mass Transfer **11** (2018), 30.